University of California
Los Angeles

A General Theory of Wireless Power Transfer via Inductive Links

A thesis submitted in partial satisfaction
of the requirements for the degree
Master of Science in Electrical Engineering

by

Jiacheng Pan

2015

Abstract of the Thesis

A General Theory of Wireless Power Transfer via Inductive Links

by

Jiacheng Pan

Master of Science in Electrical Engineering

University of California, Los Angeles, 2015

Professor Asad A. Abidi, Chair

This thesis presents a comprehensive theory of wireless power transfer via inductive links. Design-oriented analysis is used to offer a different and insightful perspective. This thesis analyzes different architectures of wireless power transfer and different ways to realize stable power delivery over distance variations. Among various techniques for maintaining stable power delivery, a frequency-adapting architecture is proposed and implemented, in which an oscillator is used as the driver as compared with the traditional implementation of using power amplifier as the driver. The experimental results indicate that oscillator driven wireless power transfer system could self-tune to the optimal frequency and maintain stable power delivery over distance variation at a high power transfer efficiency.

The thesis of Jiacheng Pan is approved.

Dejan Marković

William Kaiser

Asad A. Abidi, Committee Chair

University of California, Los Angeles

2015

To my grandparents

Table of Contents

List of Figures

Acknowledgments

I would like to express my deepest gratitude to Professor Asad Ali Abidi who has guided me with patience and wisdom since the time I took EE10 at my college Sophomore year. He is the best advisor I've ever had in my career. It is him who enlightened me of the beauty of electric circuits and brought me into this fascinating world of electronics. It is him who taught me how to think intelligently and intuitively. And it is him who strengthened my will to dedicate my life to the pursuit of wisdom.

I would like to thank Professor Dejan Marković for offering me a great opportunity to integrate my wireless power transfer system with his implantable brain device system. It would always be thrilling to see theories being transformed into real-life applications. I am very grateful for his help.

I would also like to thank Professor William Kaiser for being on my thesis committee and offering precious advice to me. I am truly thankful for his generous help on the development of my work.

Weiyu Leng offered me great advice and guidance on how to select wires and pick the right geometry to design inductors with high quality factors. I am very grateful for his help.

CHAPTER 1

Introduction

1.1 Background of this Research

Wireless power transfer has become an emerging hot topic for various applications. As wireless communication technology matures, people are beginning to research on wireless power transfer to "cut the last wire". Wireless power transfer via strongly coupled magnetic resonances was first proposed in 2007[1]. Unlike previously designed wireless power transfer systems, the resonance-based wireless power transfer system was designed to have the power transmitter and receiver resonating at the same frequency, so that the natural power of resonance was excited so that energy could be transferred more efficiently.

As further research was conducted on resonance-based wireless power transfer, various effects were detected and analyzed. It has been discovered that optimal operating frequency for wireless power transfer is not necessarily the resonance frequency, and there is a "frequency-split" effect as the distance between coupled inductors got closer[2]. It has also been discovered that a multiple-coil configuration helps improve the power transfer efficiency[3][4]. Various models have been proposed for wireless power transfer systems. For example, a feedback-based model[5] was developed to explain various effects in wireless power transfer.

1.2 Contribution of this Work

This work develops a theory that leads to a comprehensive and design-oriented understanding of wireless power transfer systems and an elegant model that graphically explains the mechanisms in wireless power transfer via inductive links. Publications on the subject

date back to the 1970s, but each has contributed pieces to the overall picture. A common criticism of existing analyses is that they are opaque and overly-complicated, seemingly useful only to their authors. The work presented in this dissertation was developed from fundamental principles. However, it offers deep and powerful insights.

This work also offers optimization strategies that actually work. It focuses on optimization towards high efficiency in power transfer, and stable power delivery over distance variations, which are the two key factors that people have been struggling with for years to improve. At the end, a prototype system was implemented and tested to validate the theory presented in this work.

1.3 Organization of this Thesis

In this thesis, a general theory and model of wireless power transfer is discussed in Chapter 2. A prototype circuit implemented to validate the theory is presented in Chapter 3. Finally, Chapter 4 concludes this thesis.

CHAPTER 2

A General Theory of Wireless Power Transfer through Inductive Links

2.1 System Overview

Like any power transfer system, inductive link based wireless power transfer systems have the following general structure: The system starts with a power transmitter where all the power originates (source). It is then followed by a power transfer link through which power could flow from source to load. At the end is a power receiver which harvests power from the link and delivers it to the load.

An example of the system structure (Fig. 2.1) is a wired power transfer system. The electric grid system transfers power from a power plant to thousands of households. For that power transfer system, power transmitter is the power plant where all the power originates. Power transfer link is the electric grid system that is composed of transmission lines, transformers, etc. Power receivers are the electric devices that are plugged into outlets to consume power.

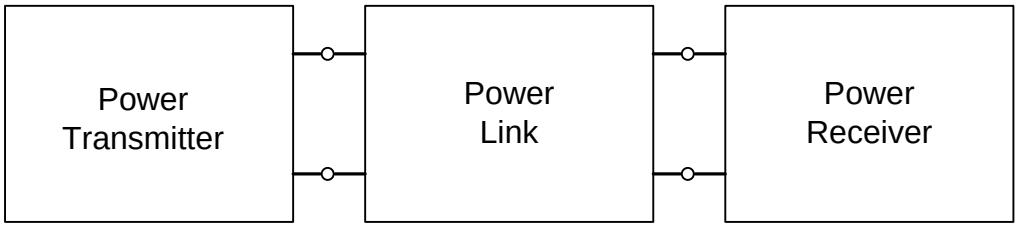

Figure 2.1: Power transfer system structure.

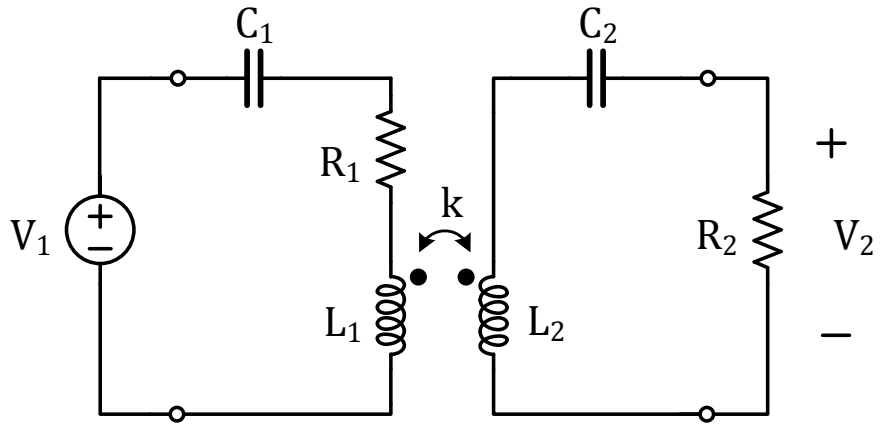

Figure 2.2: Series-LCR circuit.

2.2 Power Transfer Link Analysis

2.2.1 Series-LCR and Parallel-LCR Power Links

For simplicity of analysis, details of power transmitters and power receivers are ignored for now. Power receivers consume energy that is delivered, so it is assumed here that power receiver is a constant resistor. Power transmitters are the energy sources, and real-life power transmitters are of different manifestations. However, they could be equivalently treated as voltage sources, current sources, or combinations of both. For example, one of the simplest forms of energy sources is a battery, and a battery is equivalently a voltage source followed by a series resistor. Another example is an LC oscillator, a simple LC oscillator is constructed by a cross-coupled FET pair followed by an LC-tank; the cross-coupled FET pair is the energy source and the equivalent circuit for that is a current source. As a result, it is assumed here that power transmitter is either a voltage source or a current source.

Having made the above assumptions, two types of inductive links are of interests. For a voltage source power transmitter, a series combined LCR power link is considered. For a current source power transmitter, a parallel combined LCR power link is considered.

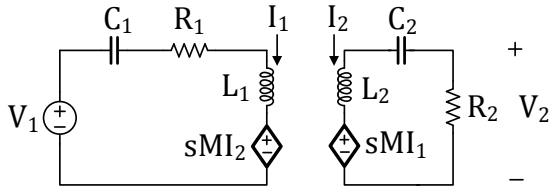

Figure 2.3: Series-LCR equivalent circuit.

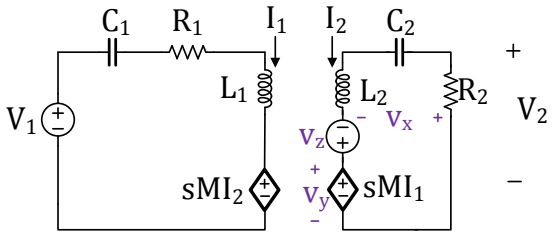

Figure 2.4: The Dissection Theorem for series-LCR circuit.

2.2.2 A "Q-Tip" Theory for Series-LCR Coupled Resonators

The analysis of power transfer link is first conducted on series-LCR case and then extended to other cases.

A series-LCR coupled resonator has a prototype circuit as shown in Fig. 2.2. Note that power transmitter is modeled as a voltage source V_1 and power receiver is modeled as a constant resistor R_2 so that all the focus is on the link.

It is a fourth-order system. If traditional circuit analysis methods such as node voltage method or loop current method is adopted, a 4×4 matrix would be formed and the result would be some bulky and complicated expression. In order to get concise equations that reveal the essence of the circuit and offer design intuition, the Dissection Theorem[6][7][8] is applied so that low-entropy expression could be derived.

Before applying the Dissection Theorem, an equivalent circuit which replaces the inductor coupling with current-controlled voltage source (CCVS) is built. (Fig. 2.3)

The first step of "Dissecting" the circuit is to inject a stimulus without perturbing the network. As shown in Fig. 2.4, an independent voltage source (v_z) is injected. Then following from the Dissection Theorem, the transfer function is:

$$H = \frac{V_2(s)}{V_1(s)} = H^{u_y} \frac{1 + \frac{1}{T_n}}{1 + \frac{1}{T}} \tag{2.1}$$

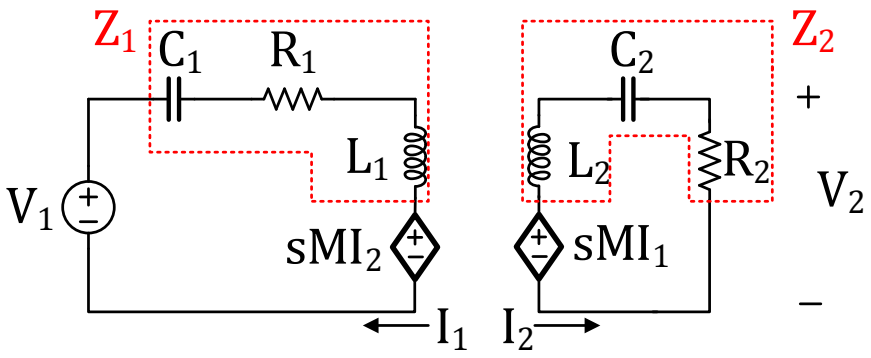

Figure 2.5: Visualization of Z_1 and Z_2.

with

$$H^{u_y} = \frac{V_2(s)}{V_1(s)}\bigg|_{v_y=0} = \frac{-I_2(R_2 \| \frac{1}{sC_2})}{sM \cdot I_2} = -\frac{R_2 \| \frac{1}{sC_2}}{sM} \tag{2.2}$$

$$T_n = \frac{v_y(s)}{v_x(s)}\bigg|_{V_2=0} = \frac{sM \cdot I_1}{0} = \infty \tag{2.3}$$

$$T = \frac{v_y(s)}{v_x(s)}\bigg|_{V_1=0} = \frac{sM \cdot I_1}{-\frac{I_1 \cdot Z_1}{sM} \cdot Z_2} = \frac{-(sM)^2}{Z_1 \cdot Z_2} \tag{2.4}$$

where $Z_1(s) = 1/sC_1 + R_1 + sL_1$ and $Z_2(s) = 1/sC_2 + R_2 + sL_2$ are the series impedances as shown in the dashed boxes in Fig. 2.5.

From the knowledge of Input/Output Impedance Theorem[6][7][8], the total input impedance seen at the V_1 port could be calculated as:

$$Z_{in}(s) = (Z_{in}\big|_{T=0}) \cdot (1 + T). \tag{2.5}$$

T has been calculated already, and $Z_{in}\big|_{T=0}$ is just the input impedance when there is no coupling between the two inductors L_1 and L_2, because $T = 0$ indicates $M = 0$, the mutual inductance is 0. As a result, $Z_{in}\big|_{T=0} = Z_1$.

Equivalently, the circuit could be drawn as a source V_1 driving an impedance $Z_1(s)$ in series with a transformed impedance $Z_T(s)$ that is dependent on the rest of the circuit (Z_2 and M) (Fig. 2.6).

$Z_1(s)$ is the original L_1, C_1 and R_1 associated with the transmitter-side network. $Z_T(s) = Z_1 \cdot T = \frac{-s^2k^2L_1L_2}{Z_2}$ is effectively the impedance looking at the port over the left controlled

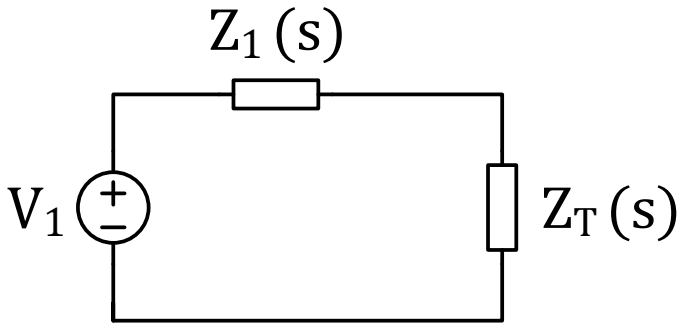

Figure 2.6: Transformed impedance for series-LCR.

source sMI_2. Looking into that port from left to right, the only energy-dissipating element is the load R_2. As a result, it could be concluded that energy dissipated in $Z_1(s)$ is the energy wasted in source impedance, and energy dissipated in $Z_T(s)$ is the energy delivered to the load[5].

Having derived an elegant equivalent circuit for the series-LCR, power transfer characteristic is of interest. In real-life application, power delivery metrics include maximum power transfer, power transfer efficiency, stable power delivery, etc. The following power transfer analysis starts from maximum power transfer analysis and incorporates the analysis of power transfer efficiency and conditions for stable power delivery (which is important for wireless power transfer applications as compared with wired power transfer cases) as the analysis evolves.

To maximize the power delivered to the load at sinusoidal steady state, the following condition needs to be satisfied:

$$Z_1(j\omega) = Z_T(j\omega)^* \quad \Rightarrow \quad Z_1(j\omega) = \left[\frac{\omega^2 k^2 L_1 L_2}{Z_2(j\omega)}\right]^*, \tag{2.6}$$

which is equivalent to the following two conditions:

$$\left|Z_1(j\omega)\right| = \left|\frac{-(j\omega)^2 k^2 L_1 L_2}{Z_2(j\omega)}\right| \quad \Rightarrow \quad \left|\frac{Z_1(j\omega)}{j\omega L_1}\right| = k^2 \left|\frac{j\omega L_2}{Z_2(j\omega)}\right|; \tag{2.7}$$

$$\angle Z_1(j\omega) = -\angle\left[\frac{-(j\omega)^2 k^2 L_1 L_2}{Z_2(j\omega)}\right] \quad \Rightarrow \quad \angle Z_1(j\omega) = \angle Z_2(j\omega). \tag{2.8}$$

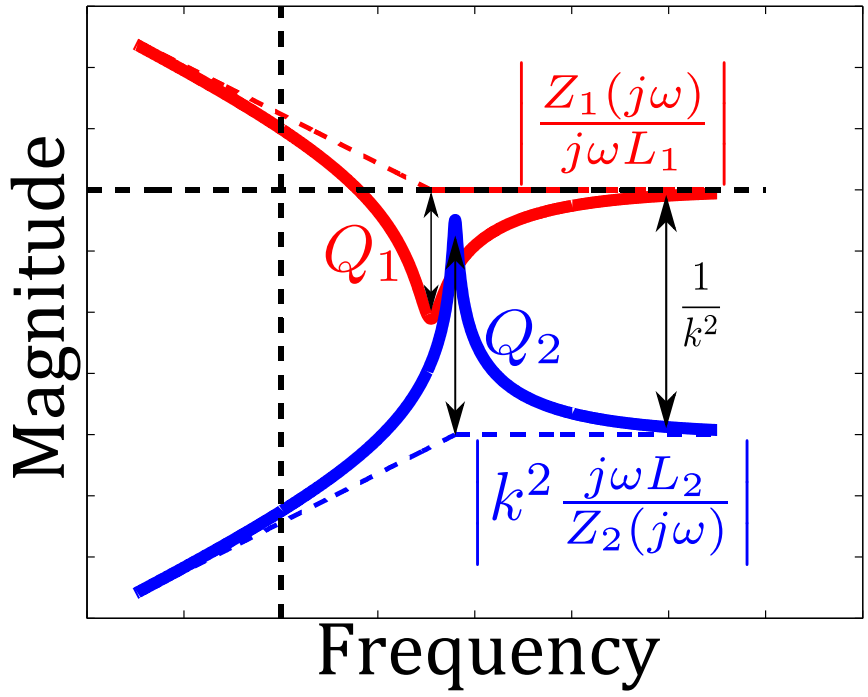

Figure 2.7: A general "Q-tip" diagram (graphical representation of eq. 2.7).

A graphical representation for equation 2.7 is shown in Fig. 2.7. The condition $\left|\frac{Z_1(j\omega)}{j\omega L_1}\right| = k^2\left|\frac{j\omega L_2}{Z_2(j\omega)}\right|$ for maximum power transfer is manifested as two "Q-curves" intersecting on the graph. From Fig. 2.7 two conclusions can be drawn:

1. It's desirable to design the two parts of networks to have the **same resonance frequencies**. In that case, the "tips" of the Q-curves (later referred to as "Q-tips") are aligned and the two Q-tips are able to touch at smaller coupling coefficient k which means longer distance separation.

2. It's desirable to design the two resonators to have as **large quality factors** as possible. The larger the quality factors, the further the "Q-tips" could reach.

The second condition for maximum power transfer, $\angle Z_1(j\omega) = \angle Z_2(j\omega)$ (eq. 2.8), is shown on Fig. 2.8. If the two "Q-curves" have different quality factor values, the only point where $\angle Z_1(j\omega)$ and $\angle Z_2(j\omega)$ could be equal is at resonance frequency ω_0. However, if Z_1

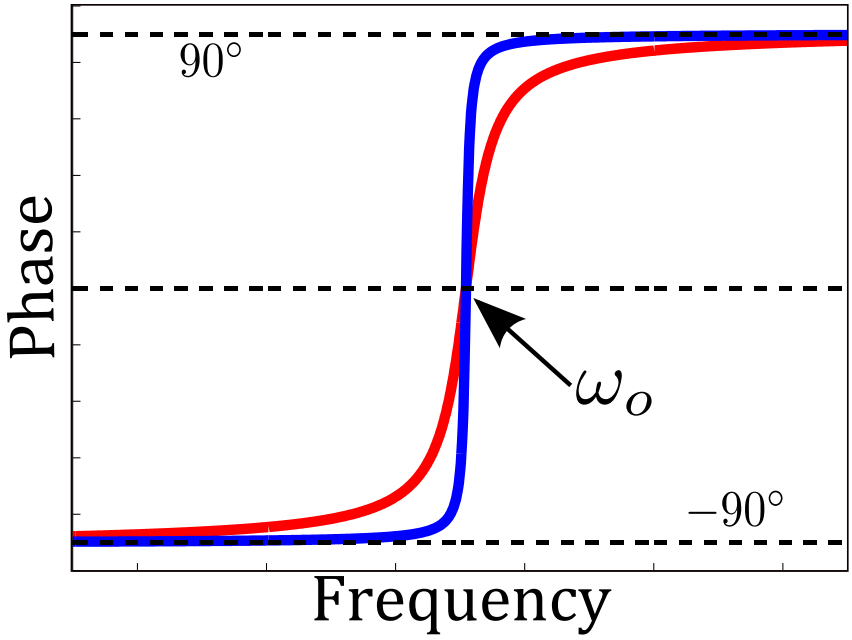

Figure 2.8: A general "Q-tip" diagram(phase) (graphical representation of eq. 2.8).

and Z_2 have the same quality factors, the two curves completely coincide, meaning that the angles are equal to each other all the time.

Besides the two conclusions drawn above, there is an additional one:

3. For maximum power transfer condition to be satisfied at different coupling coefficients, it's desirable to have **equal quality factors**: $Q_1 = Q_2$.

To sum up, in order to achieve maximum power transfer for the system, it is desired to set the two parts of the network to have the same resonance frequencies($\omega_{res,1} = \omega_{res,2}$), the same quality factors($Q_1 = Q_2$), and as large quality factors as possible($Q_1, Q_2 \gg 1$). A system meeting the requirements would transfer power in the following three different scenarios depending on the value of the coupling coefficient k.

1. Under-coupled: When $k^2 < \frac{1}{Q_1 Q_2}$, the "Q-tips" never touch. The system will never meet the maximum power transfer conditions.

2. Critical-coupling: When $k^2 = \frac{1}{Q_1 Q_2}$, the "Q-tips" touch at the tips. The system meets

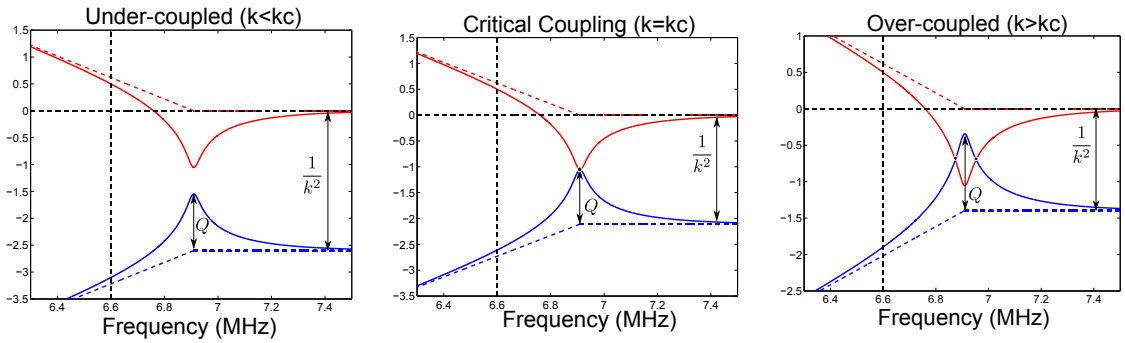

Figure 2.9: The "Q-tip" diagram for three different cases.

the maximum power transfer conditions at resonance frequency.

3. Over-coupled: When $k^2 > \frac{1}{Q_1 Q_2}$, the "Q-tips" intersect at two points. The system meets the maximum power transfer conditions at those two frequencies where "Q-tips" touch each other.

The critical coupling coefficient is defined as:

$$k_c \triangleq \sqrt{\frac{1}{Q_1 Q_2}}, \tag{2.9}$$

and Fig. 2.9 shows all three cases.

2.2.3 An Extended "Q-Tip" Theory for Series-LCR Coupled Resonators

In real-life circuit design, it is possible to design two resonators to have the same resonance frequencies by tuning their LC products. Also, by picking elements with little loss, it is possible to have high-Q systems. However, it is unrealistic to have exactly the same Q for the two resonators. The extended "Q-tip" Theory explains what happens when two resonators have unequal Q's.

First, recall that when the two resonators have the same quality factors, maximum power transfer happens at "Q-tip" intersection points. And at those frequencies, the equivalent circuit looks like two equal resistors in series. (Fig. 2.10 $Z_1(s)$ becomes R_1 and $Z_2(s)$ becomes $R_T = R_1$) In other words, $Imag\{Z_1\}$ cancels $Imag\{Z_T\}$.

Now, keep the operating frequency unchanged and change the value of R_1. Note that

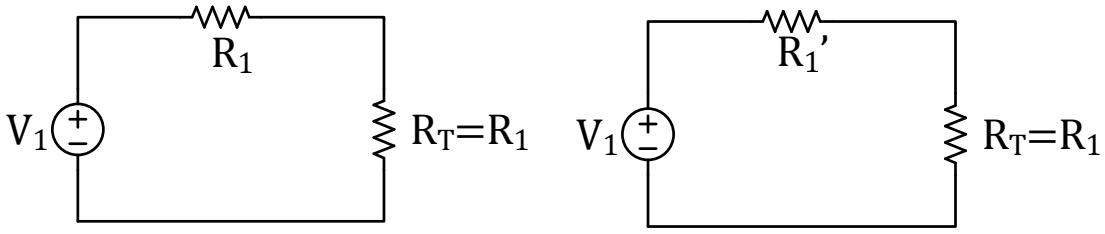

Figure 2.10: The equivalent circuit at "Q-tip" intersecting frequencies for equal Q (left) and unequal Q (right).

$Imag\{Z_1\}$ has nothing to do with R_1, and $Imag\{Z_T\}$ does not change with R_1 because $Z_T = \frac{-s^2k^2L_1L_2}{Z_2}$ has nothing to do with R_1 as well. In fact, the circuit will still be purely resistive, and variation of R_1 only affects the power transfer efficiency. The smaller R_1 gets, the more efficient the power transfer is.

Moreover, notice that for any given system, at "Q-tip" intersecting frequencies, the equivalent circuit would look like R_1 in series with a R_T, and that R_T will stay constant as long as the circuit components stay unchanged. With a constant driver V_1, it means that **stable power** is delivered to the load regardless of coupling coefficient variation which is mainly due to distance variation.

To conclude, for any series coupled resonators with equal resonance frequencies and sufficiently large quality factors:

1. The system is purely resistive at "Q-tip" intersecting frequencies (if there is any). To construct the "Q-tip" diagram, Q_2-curve stays as it is, and Q_1-curve should be modified: R_1 is chosen so that Q_1 is equal to Q_2.

2. At "Q-tip" intersecting frequencies, if V_1, the driver, has a constant driving strength, then stable power is delivered to the load regardless what the coupling coefficient k between the two inductors is (as long as it's greater than k_c, the critical coupling coefficient).

3. The power transfer efficiency would be:

$$\eta = \frac{R_T}{R_T + R_1'} \times 100\%. \tag{2.10}$$

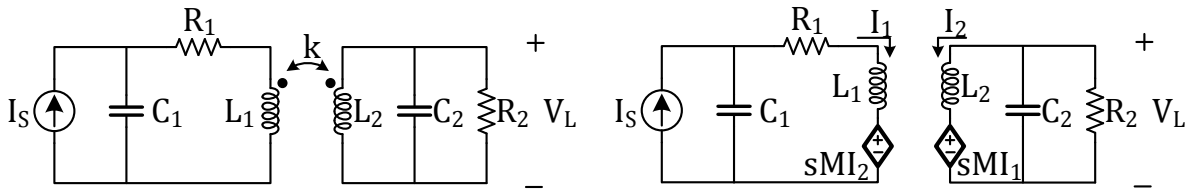

Figure 2.11: The parallel-LCR coupled resonator circuit (left) and its equivalent circuit (right).

2.2.4 "Q-Tip" Theory for Parallel-LCR Coupled Resonators

Having gotten the "Q-tip" Theory for series-LCR case, it is not hard to extend that to parallel-LCR coupled resonators (Fig. 2.11[1]). Unlike series-LCR circuits to which the controlled voltage source equivalent circuit of coupled inductors add no extra complexity, parallel-LCR coupled resonators, after replacing coupled inductors with their equivalent circuits, seems hard to analyze. Again, the Dissection Theorem will be applied so that low-entropy forms could be achieved.

First of all, coupled inductors are replaced with uncoupled inductors in series with current-controlled voltage sources (Fig. 2.11). This construction of equivalent circuit allows the Dissection Theorem to be applied fluently (the voltage injection could be in series with one of the controlled voltage source).

Then applying the Dissection Theorem (Fig. 2.12), it could be calculated that:

$$H = \frac{V_L(s)}{I_S(s)} = H^{u_y} \frac{1 + \frac{1}{T_n}}{1 + \frac{1}{T}}, \tag{2.11}$$

[1]The reason why on the transmitter side C_1 is in parallel with L_1 and R_1 rather than all three of them are in parallel is because such configuration is a more fundamental representation of what's going on in the circuit: the Q_L (quality factor associated with inductor) is dominating over Q_C (quality factor associated with capacitor). And an equivalent circuit for real-life inductor is a series combination of inductor and resistor

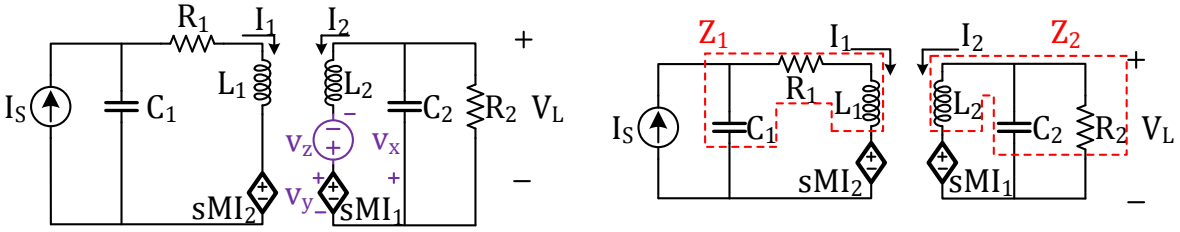

Figure 2.12: Apply the Dissection Theorem to parallel-LCR circuit (left); Visualization of Z_1 and Z_2 (right).

with

$$H^{u_y} = \left.\frac{V_L(s)}{I_S(s)}\right|_{v_y=0} = \frac{-I_2(R_2 \| \frac{1}{sC_2})}{(sM)(sC_1)\cdot I_2} = -\frac{R_2 \| \frac{1}{sC_2}}{(sM)(sC_1)}, \tag{2.12}$$

$$T_n = \left.\frac{v_y(s)}{v_x(s)}\right|_{V_L=0} = \frac{sM \cdot I_1}{0} = \infty, \tag{2.13}$$

$$T = \left.\frac{v_y(s)}{v_x(s)}\right|_{I_S=0} = \frac{sM \cdot I_1}{-\frac{I_1 \cdot Z_1}{sM} \cdot Z_2} = \frac{-(sM)^2}{Z_1 \cdot Z_2}, \tag{2.14}$$

where $Z_1(s) = 1/sC_1 + R_1 + sL_1$ and $Z_2(s) = 1/(sC_2 + G_2) + sL_2$ are the series impedance as shown in the dashed boxes in Fig. 2.12.

Now that T has been calculated, the next step would be to figure out an equivalent circuit that looks like Fig. 2.6 so that power transfer characteristics could be visualized from the circuit topology.

According to Input/Output Impedance Theorem, the input admittance to the system is:

$$Y_{in}(s) = (Y_{in}|_{T=0}) \cdot \frac{(1+T)}{1+T|_{Y_{source}=0}} = (Y_{in}|_{T=0}) \cdot \frac{(1+T)}{(1+T')}, \tag{2.15}$$

where Y_{source} is an additional admittance put right across I_S in shunt with all the other

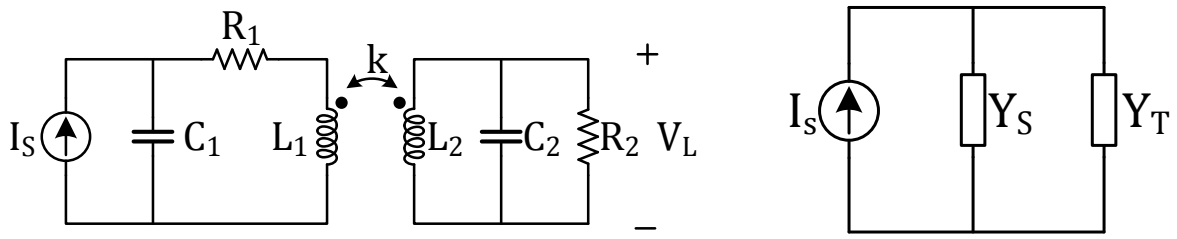

Figure 2.13: The original parallel-LCR coupled resonator circuit (left) and a 2-piece equivalent circuit for power analysis (right).

components,[2] and:

$$Y_{in}(s)\big|_{T=0} = sC_1 + \frac{1}{sL_1 + R_1}, \tag{2.16}$$

$$T(s) = -\frac{(sM)^2}{Z_1 Z_2}, \tag{2.17}$$

$$T'(s) = -\frac{(sM)^2}{(sL_1 + R_1)Z_2}. \tag{2.18}$$

Apparently the existence of the correction factor $1/(1 + T'(s))$ adds to the difficulty of coming up with a compact equivalent circuit for the purpose of power transfer analysis. To fully understand what's going on, the following analysis will start with several ideal assumptions; then those assumptions are taken out step by step like reeling silk off cocoons to reveal the complete precise look of the system.

- **Step 1**: Add assumption 1: the correction factor to input admittance $\frac{1}{1+T'} \approx 1$.

  In that case,

$$Y_{in}(s) \approx (Y_{in}\big|_{T=0}) \cdot (1 + T) = (Y_{in}\big|_{T=0}) + (Y_{in}\big|_{T=0}) \cdot T = Y_S + Y_T. \tag{2.19}$$

  The equivalent circuit looks like Fig. 2.13.

  Although Y_S is equivalently the transmitter part of the circuit without any coupling to the receiver part, one question that needs to be asked is: Is the power delivered to Y_S in the equivalent circuit the same to the power delivered to R_1 in the original circuit?

[2] As compared with series-LCR circuit, there is an extra $\frac{1}{1+T\big|_{Y_S=0}}$ term. The reason why this term does not exist in series-LCR is because $T\big|_{Z_S=0} = 0$ for series-LCR resonators

(Similarly, is the power delivered to Y_T the same as the power delivered to R_2?) To figure it out:

First notice that due to conservation of energy, the total power dissipation in the equivalent circuit is equal to that in the original circuit:

$$P_{total,equivalent} = P_{Y_S} + P_{Y_T} \text{ with } P_{Y_S} = \frac{\left|V_S\right|^2}{2\omega^2 {L_1}^2/R_1}, \tag{2.20}$$

$$P_{total,original} = P_{R_1} + P_{R_2} \text{ with } P_{R_1} = \frac{1}{2}\left|I_1\right|^2 R_1, \tag{2.21}$$

where I_1 and I_2 are the currents through L_1 and L_2 in the original circuit respectively, and V_S is the voltage across Y_S in the equivalent circuit.

Also, applying Kirchhoff's Voltage Law to the original circuit,

$$\begin{cases} V_S = (sL_1 + R_1)I_1 + (sM)I_2 \\ -\frac{I_2}{sC_2+G_2} = sL_2 \cdot I_2 + sM \cdot I_1 \end{cases} \Rightarrow V_S = (sL_1 + R_1) \cdot I_1 - \frac{(sM)^2}{Z_2} \cdot I_1, \tag{2.22}$$

a relation between V_S and I_1 could be derived for the original circuit. Moreover, the voltage drop across the input port, V_S, for both the original circuit and the equivalent circuit are the same.

Therefore, the relation between power into Y_S and power into R_1 is:

$$\frac{P_{Y_S}}{P_{R_1}} = \frac{\left|V_S\right|^2}{\left|I_1\right|^2 \cdot \left|sL_1\right|^2} = \left|1 - \frac{(sM)^2}{(sL_1 + R_1)(Z_2)}\right|^2 = \left|1 + T'\right|^2. \tag{2.23}$$

The total energy dissipated in R_1 is not equal to the total energy dissipated in Y_S, nor is that the case for R_2 and Y_T. In fact, the energy dissipation in Y_S and R_1 differ by a ratio of $\left|1+T'\right|^2$. And that difference also appears in the energy dissipation in Y_T and R_2 due to energy conservation.

- **Step 2**: Add assumption 2: the correction factor to power delivery $\left|1 + T'\right|^2 \approx 1$ (power "wasted" in Y_S equals to that in R_1 and power delivered to Y_T equals to that to R_2).

  The circuit now has become a dual to series-LCR resonators. Everything of the "Q-tip" Theory for series-LCR could be applied to parallel-LCR. The conclusion based on the "Q-tip" Theory is:

1. Stable power delivery happens at the point(s) where the "$\left|\frac{Y_S(j\omega)}{j\omega C_1}\right|$-curve" (the value of R_1 chosen in a way that the transmitter-side LCR has the same quality factor as the receiver-side LCR) and the "$k^2\left|\frac{j\omega L_2}{Z_2(j\omega)}\right|$-curve" intersect each other. At stable power delivery frequencies, the system is purely resistive.

2. The stable power delivery frequencies (when $k > k_c$) could be calculated based on the "Q-tip" diagram:

$$\left|\frac{(\omega/\omega_0)^2}{[1-(\omega/\omega_0)^2]+(j\omega)/(\omega_0 Q)}\right| = 1, \tag{2.24}$$

$$\Rightarrow \omega_1, \omega_2 \approx \frac{\omega_0}{\sqrt{1\pm k}} \quad \text{if } Q \gg 1. \tag{2.25}$$

3. The power transfer efficiency is:

$$\eta = \frac{Q_1}{Q_1+Q_2} \times 100\%. \tag{2.26}$$

- **Step 3**: Remove assumption 1.

  Now that the stable power delivery frequencies are calculated, it is of great interest to know what would be the influence of the admittance correction factor on the system at those frequencies.

  The admittance correction factor $= \frac{1}{1+T'(j\omega)}$, with

$$T'(j\omega) = \frac{\omega^2 k^2 L_1 L_2}{(j\omega L_1 + R_1)(Z_2)} \tag{2.27}$$

$$= \frac{\omega^2 k^2 L_1 L_2}{(j\omega L_1 + R_1)(j\omega L_2 + \frac{1}{G_2 + j\omega C_2})} = \frac{\omega^2 k^2 L_1 L_2}{-\omega^2 L_1 L_2 + j\omega R_1 L_2 + \frac{j\omega L_1 + R_1}{j\omega C_2 + G_2}} \tag{2.28}$$

$$(\text{if } Q \gg 1) \approx \frac{\omega^2 k^2 L_1 L_2}{(-\omega^2 L_1 L_2 + \frac{L_1}{C_2}) + j\omega R_1 L_2} = \frac{\omega^2 k^2}{(-\omega^2 + \frac{1}{L_2 C_2}) + j\omega \frac{R_1}{L_1}} \tag{2.29}$$

$$= \frac{k^2}{(\frac{\omega_0^2}{\omega^2}) + j\frac{1}{Q_1}}. \tag{2.30}$$

$$\tag{2.31}$$

  At stable power delivery frequencies ($\omega_1, \omega_2 \approx \frac{\omega_0}{\sqrt{1\pm k}}$),

$$T'(j\omega) = \frac{k^2}{[(1\pm k)-1] + \frac{j}{Q_1}} = \frac{k^2}{(\pm k) + \frac{j}{Q_1}}. \tag{2.32}$$

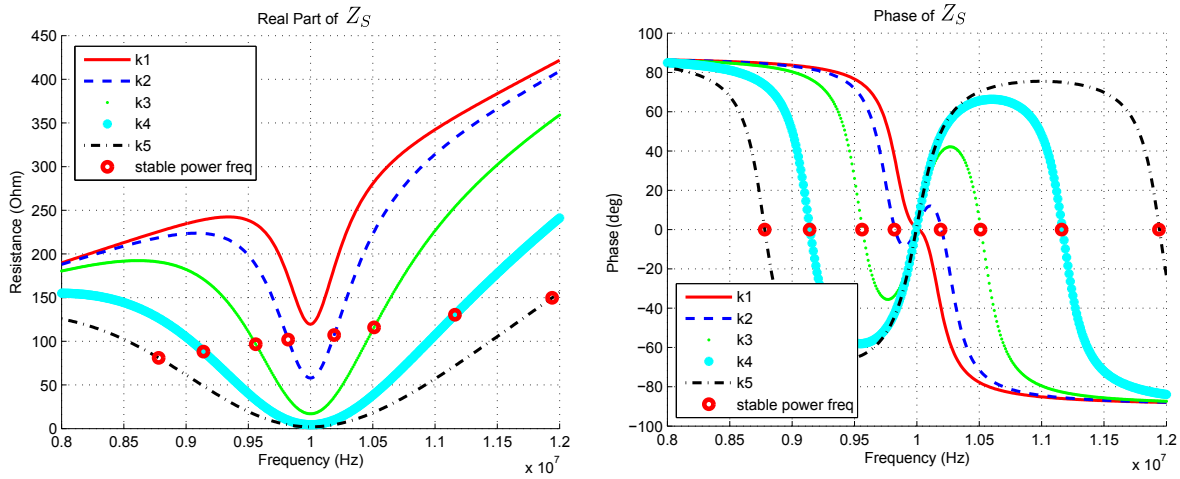

Figure 2.14: To amplify the differences, $Z_S = 1/Y_S$ is plotted. $k_1 < \mathbf{k_c} < k_2 < k_3 < k_4 < k_5$. Red circles are the stable power delivery frequencies for different k's. In this plot, the effects of admittance correction factor has not been considered.

Then, what's the impact of $\frac{1}{1+T'(j\omega)}$ at stable power delivery frequencies?

$$\begin{cases} \text{If } k \gg \frac{1}{Q_1}\,(\omega_1, \omega_2 \text{ far from } \omega_0), & T'(j\omega) = \pm k \\ \text{If } k \ll \frac{1}{Q_1}\,(\omega_1, \omega_2 \text{ close to } \omega_0), & T'(j\omega) = \frac{Q_1 k^2}{j} \ll \frac{k}{j} \end{cases}$$

It could be seen that $\frac{1}{1+T'(j\omega)}$ has almost no influence over phase in either case. In terms of magnitude, only when k is large (stable power delivery frequencies far from the resonance frequency), $\left|\frac{1}{1+T'(j\omega)}\right|$ scales the magnitude by $\approx \frac{1}{1\pm k} = (\frac{\omega_{1,2}}{\omega_0})^2$.

Graphical illustration of the effect of the admittance correction factor is shown in Fig. 2.14, 2.15, and 2.16.

In general, for $Y_{in} = \frac{Y_S + Y_T}{1+T'}$ at stable power delivery frequencies,

$$\begin{cases} \angle Y_{in} & \approx \angle(Y_S + Y_T) = 0 \\ |Y_{in}| & = \left(\frac{\omega}{\omega_0}\right)^2 \cdot |Y_S + Y_T| = \left(\frac{R_1}{\omega_0^2 L_1^2}\right)\left(1 + \frac{Q_1}{Q_2}\right) = constant \end{cases}$$

- **Step 4**: Re-examine the power correction factor's influence and remove assumption 2.

  When taking into consideration the admittance correction factor, the equivalent circuit should be modified. The admittance correction factor scales magnitude yet doesn't

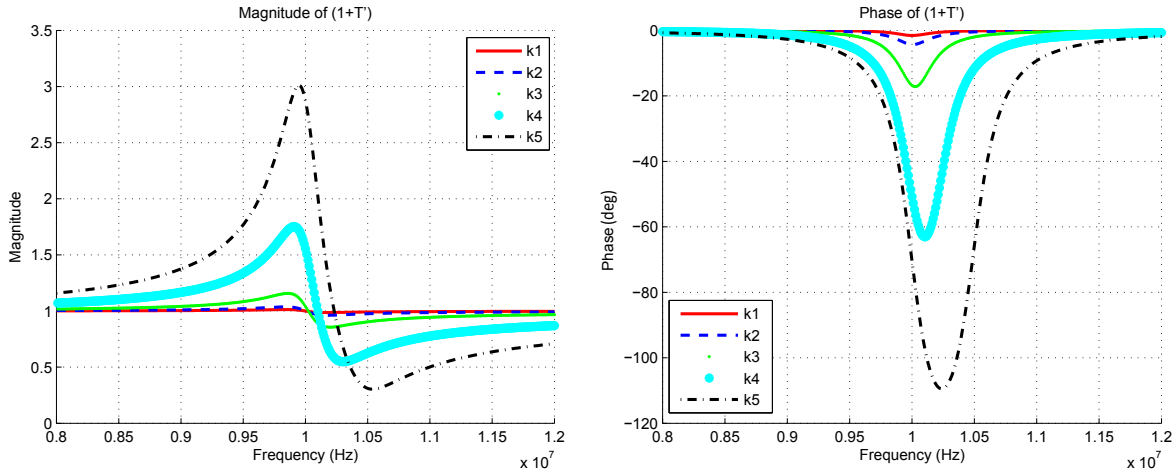

Figure 2.15: Plots of the admittance correction factor. $k_1 < \mathbf{k_c} < k_2 < k_3 < k_4 < k_5$. As could be seen on the plots, this correction factor may have some influence over magnitude, but it has negligible influence on phase at frequencies of interests.

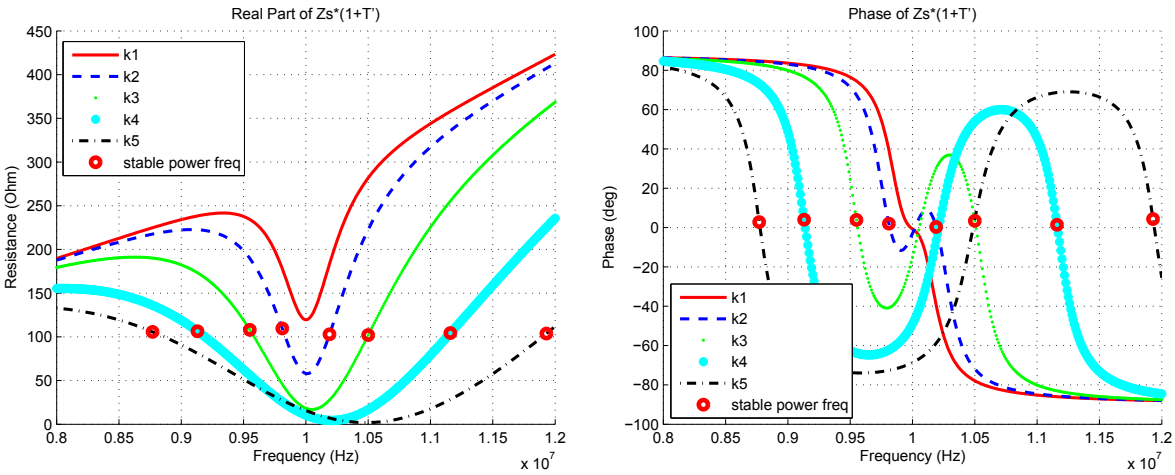

Figure 2.16: Plots of the "corrected Z_S". $k_1 < \mathbf{k_c} < k_2 < k_3 < k_4 < k_5$. As could be seen on the plots, the phase is almost unaffected; the magnitude is scaled in favor of making it a constant value over different k's.

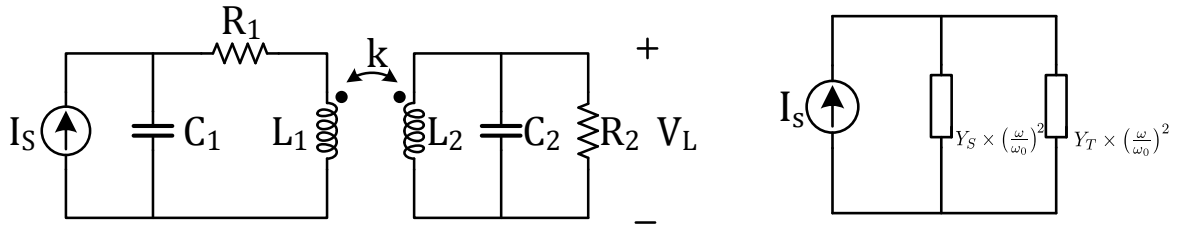

Figure 2.17: The original parallel-LCR coupled resonator circuit (left) and a 2-piece modified equivalent circuit for power analysis (right).

have any influence over phase. Therefore, the modified equivalent circuit should just have Y_S and Y_T scaled by $\left(\frac{\omega}{\omega_0}\right)^2$ (Fig. 2.17).

Re-examining the power correction factor's influence, it could be seen that the new power correction factor, $\left(\frac{P_{Y_S}}{P_{R_1}}\right)'$ has the following expression:

$$\left(\frac{P_{Y_S}}{P_{R_1}}\right)' = \frac{P_{Y_S}}{P_{R_1}} \times \left(\frac{\omega}{\omega_0}\right)^2 = \frac{P_{Y_S}}{P_{R_1}} \times \left|\frac{1}{1+T'(j\omega)}\right| \tag{2.33}$$

$$= \left|1+T'(j\omega)\right|. \tag{2.34}$$

The power consumed in Y_S and in R_1 differ by a ratio of $|1+T'(j\omega)|$. Due to energy conservation, the difference in power consumed in Y_S and R_1: $\Delta_P = P_{Y_S} - P_{R_1}$ is reflected as the difference in power delivered to R_2 and Y_T:

$$P_{Y_S} - P_{R_1} = P_{R_2} - P_{Y_T}. \tag{2.35}$$

Finally, remove the assumption of power correction factor ≈ 1:

$$\text{Power "wasted" in } Y_S : P_{Y_S} = \frac{1}{2}\left|V_{in}\right|^2 \frac{R_1}{\omega_0^2 L_1^2}, \tag{2.36}$$

$$\Rightarrow\text{Power "wasted" in } R_1 : P_{R_1} = \frac{1}{2}\left|V_{in}\right|^2 \frac{R_1}{\omega_0^2 L_1^2}\left(\frac{\omega}{\omega_0}\right)^2 \approx \frac{1}{2}\left|V_{in}\right|^2 \frac{R_1}{\omega_0^2 L_1^2}\frac{1}{1\pm k}. \tag{2.37}$$

$$\text{Power "delivered" to } Y_T : P_{Y_T} = \frac{1}{2}\left|V_{in}\right|^2 \frac{R_1}{\omega_0^2 L_1^2} \times \frac{Q_1}{Q_2}, \tag{2.38}$$

$$\Rightarrow\text{Total power: } P_{total} = P_{Y_S} + P_{Y_T} = \frac{1}{2}\left|V_{in}\right|^2 \frac{R_1}{\omega_0^2 L_1^2} \times \frac{Q_1+Q_2}{Q_2}. \tag{2.39}$$

$$\Rightarrow\text{Power "delivered" to } R_2 : P_{R_2} = P_{total} - P_{R_1} = \frac{1}{2}\left|V_{in}\right|^2 \frac{R_1}{\omega_0^2 L_1^2}\left(\frac{Q_1}{Q_2} + \frac{\pm k}{1\pm k}\right). \tag{2.40}$$

To conclude for power transfer for parallel-LCR resonators:

1. Stable power delivery still happens at "Q-tip" intersecting frequencies like in series-LCR resonators. However, there will be fluctuation in power delivery proportional to $(\frac{Q_1}{Q_2} \pm \frac{k}{1 \pm k})$.

2. $Q_2 = \frac{1}{k_c}$ sets the critical coupling coefficient, the range of stable power delivery. The larger the Q_2 is, the larger the range gets.

3. A high Q_1 is desirable not only because it increases the efficiency $\eta = \frac{Q_1}{Q_1+Q_2} \times 100\%$, but also because high Q_1 helps reducing the fluctuation in power delivery when $k < k_c$ (when the system is within stable power delivery range).

2.3 Power Transmitter Analysis

Based on the knowledge of the power transfer link, power transmitter and receiver could be designed accordingly. This section (Section 2.3) and next section (Section 2.4) mainly focus on optimal design of power transmitter and receiver to meet the following goals: **stable power delivery over distance variation** and **high power transfer efficiency** (these are the two major issues people are tackling while designing wireless power transfer systems in real-life applications).

2.3.1 General Idea of Power Transmitter Design

The key idea guiding the design of power transmitter is based on the "Q-tip" intersecting diagram(Fig. 2.9). The message it conveys is that the system should always operate at the "Q-tip" intersection points. In power transmitter design, basically there are two factors that could be controlled: driving strength and operating frequency.

Although some system achieves stable power delivery by sensing the voltage at the load side and sending the information back to transmitter side so that driving strength could be adjusted to stabilize the power delivered to load, however, the problem is that such design

adds to the complexity to the system by introducing an additional data transfer link and micro-controllers that consume extra power. Also, such ideas are "dumb" in a sense that while they mechanically control the power to the load, the power transfer efficiency may end up being very low. Moreover, in some biomedical applications, the power receiver is part of the implant, and it's certainly not a good idea to make implants bulky. As a result, achieving stable power delivery by adjusting the driving strength is not a good idea.

Good designs should focus on tuning the operating frequency. A power transmitter that could tune to operate at "Q-tip" intersecting frequencies is a manifestation of good design because it requires zero knowledge from the load side but may still deliver stable power to the load efficiently.

In Zierhofer's[9][10] design, a feedback loop is introduced to a power amplifier driven wireless power transfer system. An extra inductor is introduced to effectively sense the frequency at the transmitter side. And that inductor is coupled with another one at the power amplifier driver side so that the driving frequency could be tuned. However, extra inductors add to the power loss of the system and degrade efficiency. The proposed design also didn't focus on having the same resonance frequencies for the two resonators, and based on analysis showed in the previous section, "misaligned" "Q-tips" degrade the performance.

In Sample's[2] work, the frequency splitting effect was observed and it proposed a general idea of adaptive controlling operating frequency. The problem with adaptive control is that extra digital blocks implementing adaptive control algorithms need to be added to the system. There will be extra energy loss, and the system might not react to the change in environment that fast due to the response time needed by the digital control blocks.

So is there a way that system could be automatically controlled? Is there a way that the natural force of a system could be tamed to help on forcing the system to operate at stable power delivery frequencies?

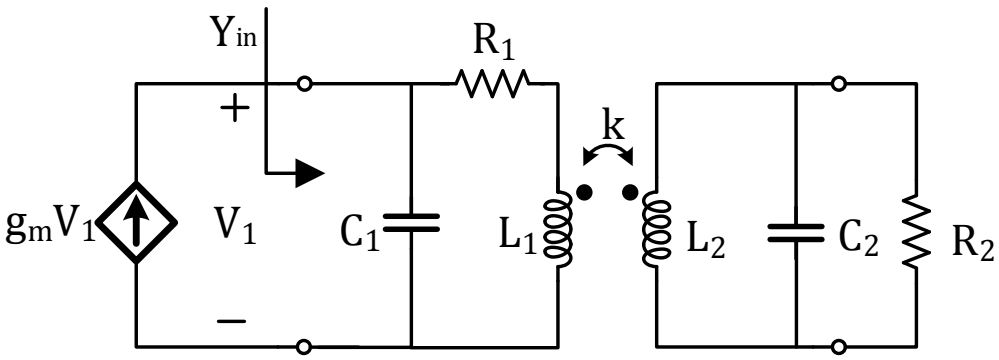

Figure 2.18: An equivalent circuit to oscillator-driven wireless power transfer system.

2.3.2 An Oscillator Based Design that Self-Tunes the Operating Frequency

For LC-oscillators(Fig. 2.18), the Barkhausen Oscillation Criterion says: The oscillator would oscillate at the frequency that makes $Im\{Y_{in}(j\omega)\} = 0$

Also, when the coupled-LCR resonators power link is at stable power delivery frequencies, the input admittance $Y_{in} = (Y_S + Y_T)(1 + T')$ is purely real as well. In other words, the requirement for oscillation and the requirement for stable power delivery coincide! The oscillator automatically tunes to the frequency that delivers stable power.

As a result, an oscillator-based wireless power transfer[11] self-tunes to the stable power frequency. If properly designed, Q_1 (the quality factor associated with the transmitter side) could be made large so that the fluctuation of power delivered could be minimized and the total system operates at high efficiency. Additionally, a low-power adaptive loop control could be introduced to regulate the amplitude at the transmitter side to ensure stable power delivery (Fig. 2.19).

In the oscillator based wireless power transfer system as shown in Fig. 2.19, parameters of the system should be chosen in the following way to meet the design specifications:

1. Q_2, the quality factor associated with the receiver part of the circuit, dictates the range of stable power delivery. Given the required range d_c, a critical coupling coefficient k_c could be calculated based on inductor coil design. While there are many different equations predicting the relation between distance and coupling coefficient, one commonly

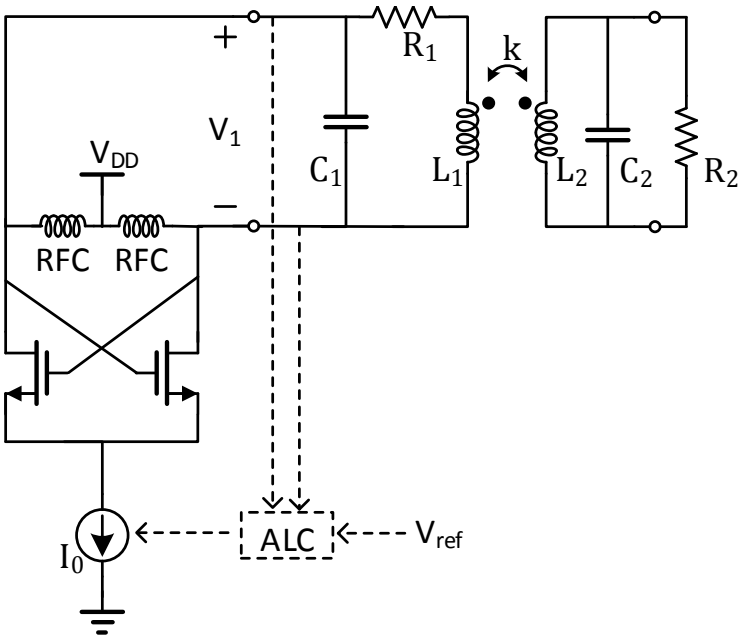

Figure 2.19: An oscillator-driven wireless power transfer system.

used equation is the Roz's formula:

$$k \approx \frac{r_1^2 r_2^2}{4\sqrt{r_1 r_2 (d^2 + r_1^2)^3}} \text{ when } r_1 \geq r_2. \tag{2.41}$$

Thus, d_c could be mapped to a k_c, and Q_2 should be chosen so that $Q_2 = \frac{1}{k_c}$.

2. Q_1, the quality factor associated with the transmitter part of the circuit, determines the power transfer efficiency as well as the fluctuation in delivered power. In general, Q_1 should be made as large as possible to minimize the fluctuation in power delivery and maximize the efficiency. The efficiency is given by

$$\eta = \frac{Q_1}{Q_1 + Q_2} \times 100\%. \tag{2.42}$$

In actual design, Q_1 is mainly determined by the quality factor of the inductor coil L_1. However, the degradation due to the oscillator driver should also be taken into account.

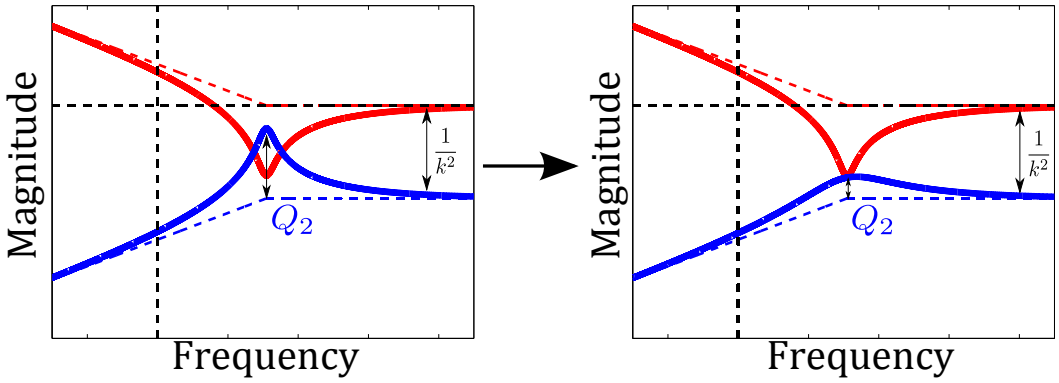

Figure 2.20: Tuning the system to optimal operating point by changing the value of Q_2.

3. At stable power delivery frequencies, the load is presented as an admittance $\approx Y_T = \frac{L_2}{L_1}\frac{1}{R_2}$ right across the source driver. Therefore, based on the requirement on power delivered to the load P_{load}, the voltage amplitude at the transmitter side should be chosen so that $\frac{1}{2}\left|V_{in}\right|^2\frac{L_2}{L_1}\frac{1}{R_2} = P_{load}$.

2.4 Power Receiver Analysis

2.4.1 General Idea of Power Receiver Design

Like the design for power transmitter, the "Q-tip" diagram reveals what could be done to have a good power receiver. Since receiver is the "passive" part of the system, operating frequency could not be controlled by the receiver. However, it could be seen that by tuning the value of the equivalent input resistance of the receiver would the quality factor of the whole receiver part of the system, Q_2, be controlled. For the sake of not harming the power transfer efficiency, the change of resistance should be done in a lossless way such as using lossless transformers, etc.

As illustrated in Fig. 2.20, a power receiver could be designed in a way that as the distance varies (k changes), Q_2 is changed in a lossless way so that "Q-tips" touch at the tips (provided that the coupling coefficient k is bigger than k_c). If this could be realized, then stable power could be delivered to the load at a constant frequency ω_0.

CHAPTER 3

An Oscillator-Driven Self-Tuning Wireless Power Transfer System that Maintains Stable Power Delivery over Distance Variation

3.1 System Overview

As described in section 2.3.2, if using an oscillator as the driver, the system would automatically be tuned to the right operating frequency so that stable power is delivered to the load. To demonstrate the power of that theory, a prototype system was implemented with discrete circuits. The prototype system used a cross-coupled FET[1] pair as the (oscillator) power transmitter, and a 470Ω resistor as the power receiver. The power transfer link used was a parallel-LCR coupled resonator circuit.

3.2 Circuit Implementation

The circuit implementation is shown in Fig. 3.1. For hand-wound coils, the inductance values are very hard to control, a little variation in the shape of coil or the winding results in a considerable amount of change in inductance. However, the beauty of the oscillator-based design is: there is no specific requirement on inductor values. The resonance frequency $\omega_0 = \frac{1}{\sqrt{LC}}$ is dependent on both inductor and capacitor, so the coils could be wound first and the only requirement is to have big quality factors. After the inductance values being measured, the capacitors could be chosen correspondingly to meet a certain resonance frequency $\omega_0 =$

[1] "Si1539CDL" was used due to small gate resistance and small drain capacitance. A data-sheet and a SPICE model could be found at "http://www.vishay.com/mosfets/list/product-67469/"

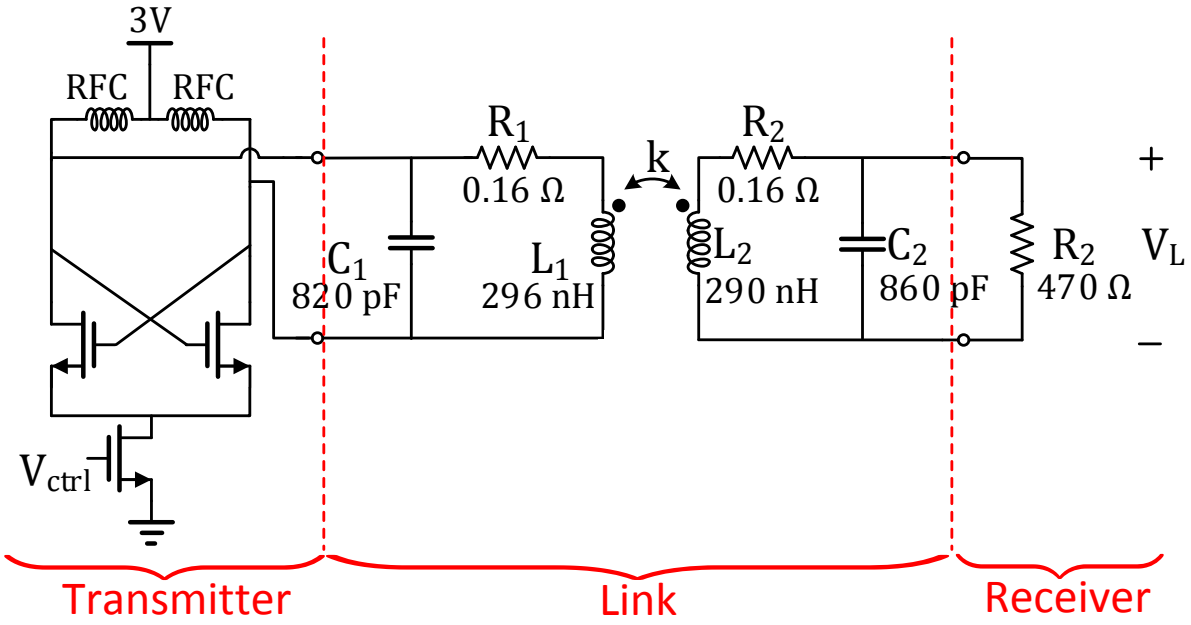

Figure 3.1: The prototype circuit implemented to verify the theory

$\frac{1}{\sqrt{LC}}$.

Two 3cm-diameter 2-turn coils wound with AWG20 wires were used as the transmitter and receiver coils. The geometry and dimension of coils were picked based on equations given by Terman[12]: The inductance[2] $L = F \times n^2 \times 2r\,(\mu H)$ for the given dimension was estimated to be on the order of several hundred nH, meaning that the capacitor that should be used was on the order of several hundred pF, which is sufficiently larger than the parasitic capacitance associated with FETs. AWG20 wires were used because the thicker the wire was, the smaller the resistance of the wire was and thus the larger the quality factor would be, and the thickest wires used in cochlear products were close to AWG20. The system was designed to work at $10MHz$, and around that frequency the coils had quality factors close to 120 which were sufficiently large. The inductances of two coils were measured to be $296nH$ for transmitter coil and $290nH$ for receiver coil. Based on the measured inductance values, capacitors were picked correspondingly so that the resonance frequency $\omega_0 = \frac{1}{\sqrt{LC}}$ was at $10MHz$. A 470Ω resistor was used to model the load. Based on the calculation of $k_c = \frac{1}{Q_2}$ and mapping to a corresponding d_c, the range of stable power delivery was around $2.5cm$.

[2]n is the number of turns; r is the radius of the coil in inch; F is dependent on the ratio of radius of coil to thickness of coil (details could be found in p.54 of [12])

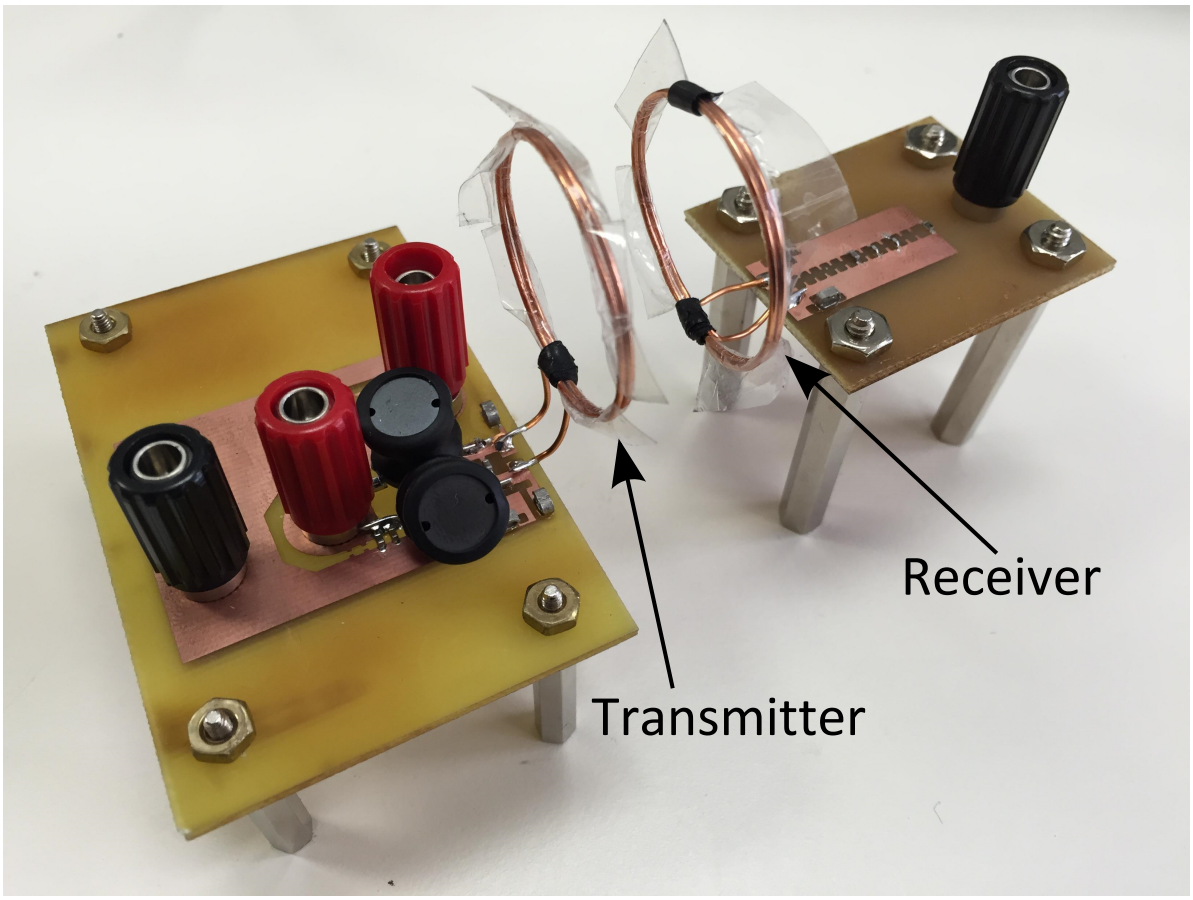

Figure 3.2: A photo of the prototype circuit

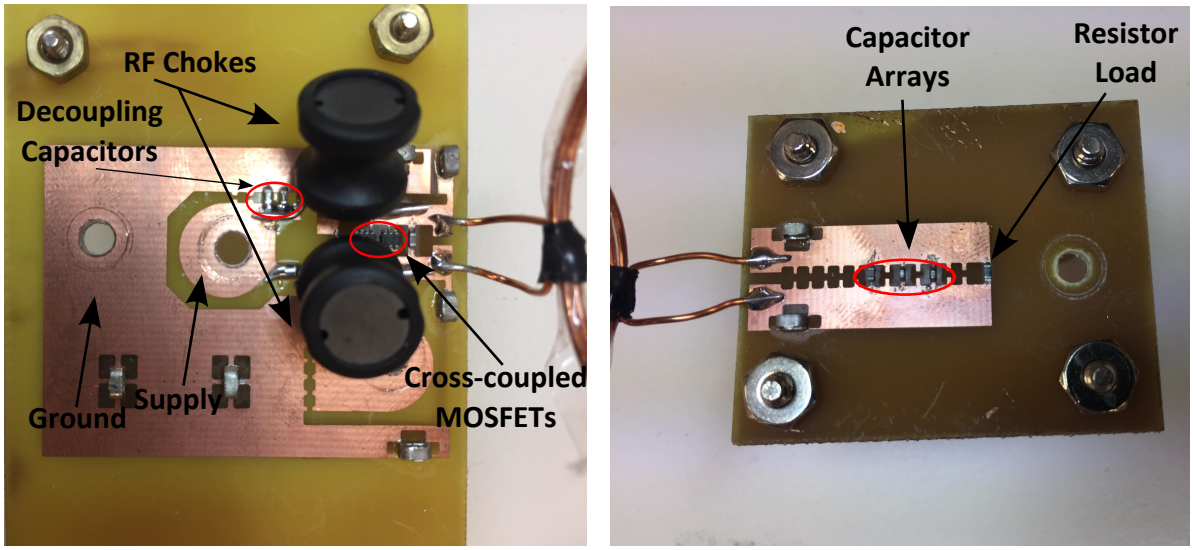

Figure 3.3: Board-level details of the transmitter (left) and receiver (right).

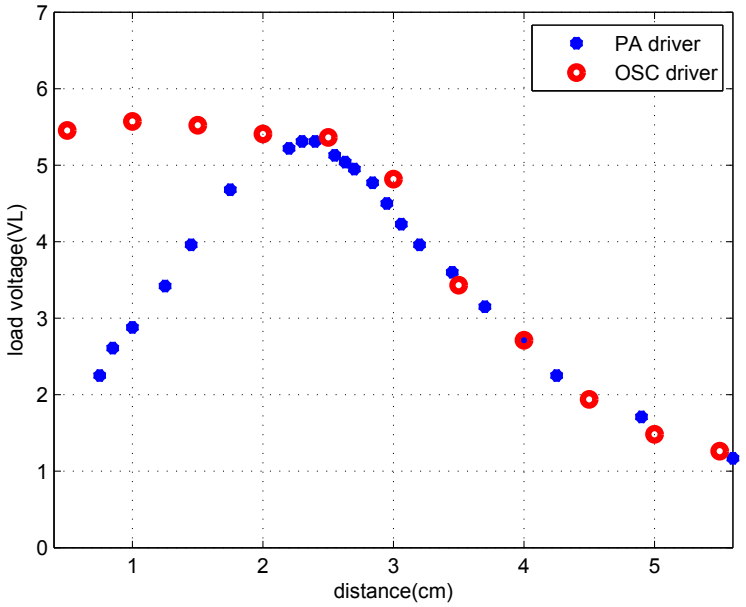

Figure 3.4: Advantage of frequency adapting design over fixed-frequency design (OSC vs. PA)

Within that range, the circuit should be able to deliver stable power to the load.

There was supposed to be an adaptive control loop that limits the amplitude of oscillation at the transmitter side so that the power to the load is fine-tuned. That amplitude control loop was not implemented in this design, but it was modelled by manually tweaking the knob of the voltage supply to the gate of the tail current FET. The "manual tweaking" captured the key of an amplitude control loop and reflected what would happen once that amplitude control loop was added.

The measurement was done under both "no amplitude control" and "manual amplitude control".

3.3 Measurements

First of all, Fig. 3.4 shows the advantage of a frequency-tuning design (in this case it's just the oscillator-based design) over a fixed-frequency design (in this case it's a power amplifier-

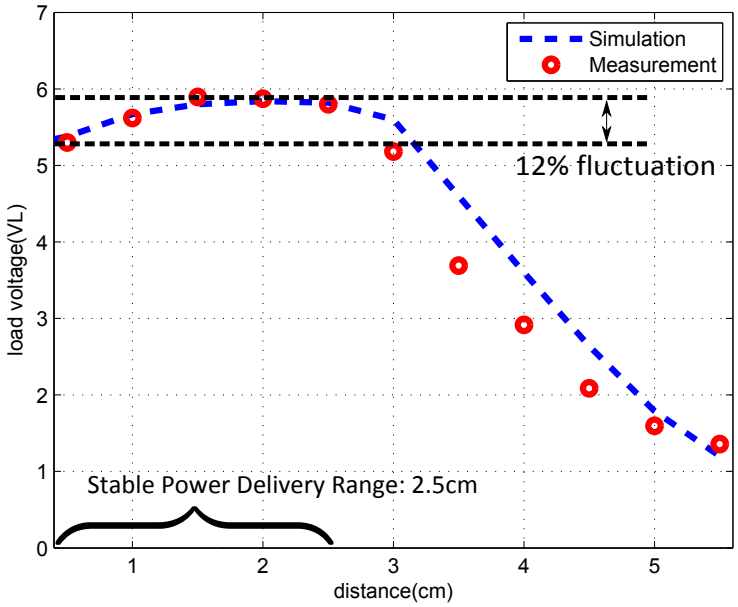

Figure 3.5: Wireless power transfer implemented using oscillator driver without amplitude control.

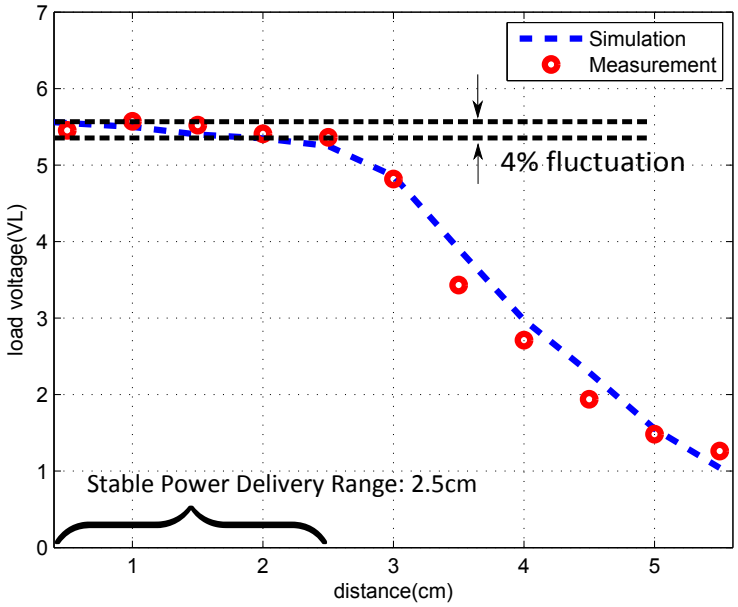

Figure 3.6: Wireless power transfer implemented using oscillator driver with amplitude control.

based design). The data for the power amplifier-based design was achieved by simulation using an ideal PA. As could be seen, for a fixed-frequency design there is only one optimal power transfer point, for any distance longer or shorter the delivered power would roll-off very quickly. However, for the oscillator-based frequency adaptive design, stable power delivery is maintained within a certain range.

Fig. 3.5 plots the simulation and measurement data for an oscillator-driven wireless power transfer system without the amplitude control loop. As could be seen on the figure, the system maintains stable power delivery within $2.5cm$ and the fluctuation in actual delivered load voltage is around 12%.

Fig. 3.6 plots the simulated and measured results for the same system yet with amplitude control. The amplitude control loop senses the oscillation amplitude at the transmitter side, compares it with a reference voltage, and regulates it to be at a constant value. As mentioned before, that amplitude control loop was not implemented. In the experiment, the oscillation voltage at the transmitter side was monitored and the tail current strength was tuned correspondingly to model the behavior of an amplitude control loop.

The power transfer efficiency for the prototype design was measured to be around 50%. One main factor that degraded the efficiency was the lossy RF-choke inductor used for this design. The RF-choke inductor had on its data-sheet a $Q = 100$, yet it turned out that $Q \approx 20$ according to measurements. If the RF-choke could be improved, then the power transfer efficiency is expected to increase to $\approx 70\%$.

In all, the prototype system operates at around $10MHz$ frequency (with $\approx 10\%$ frequency variation as the distance between transmitter and receiver varies). It delivers stable power with only 4% fluctuation within a $0 - 2.5cm$ range. It is also capable of operating at a high power transfer efficiency. The presented wireless power transfer system is very simple to be implemented because there is no need of digital controls, adaptive algorithms, etc. Nevertheless, such system is able to elegantly solve one of the biggest problems for wireless power transfer: unstable power delivery as distance separation varies. Moreover, the system achieves stable power delivery without adding to the complexity of the power receiver, and

that is essential for some biomedical applications in that small-size low-power implants are usually desired.

CHAPTER 4

Conclusion

This thesis provides a simple yet insightful model of inductive-link based wireless power transfer systems. Graphical analysis is used in addition to traditional algebraic analysis to provide an intuitive guide into design and optimization. Bulky sets of equations are simplified into beautiful curves to reveal the essence of the system: stable power delivery happens at "Q-tip" intersecting points. Two ways to enforce the intersecting of "Q-tips" are tuning the operating frequency and adjusting the quality factors, and almost all the methods of realizing stable wireless power that could be found in the literature fall into those two categories.

Moreover, an oscillator-based design is found to be elegant in that it contains an "implicit feedback loop" that auto-tunes its operating frequency to be at the right point. Unlike other ways of achieving "Q-tip" touching, the oscillator-based system is simple to be implemented; yet it is amazingly effective in transferring stable power over distance variation at high efficiency. An additional low-power amplitude control loop could be added to the given system to fine-tune the performance of wireless power transfer.

Bibliography

[1] An Kurs et al. "Wireless Power Transfer via Strongly Coupled Magnetic Resonances". In: *Science* 317.5834 (2007), pp. 83–86. DOI: 10.1126/science.1143254.

[2] A.P. Sample, D.A. Meyer, and J.R. Smith. "Analysis, Experimental Results, and Range Adaptation of Magnetically Coupled Resonators for Wireless Power Transfer". In: *IEEE Trans. on Industrial Electronics* 58.2 (2011), pp. 544–554. ISSN: 0278-0046. DOI: 10.1109/TIE.2010.2046002.

[3] A.K. RamRakhyani, S. Mirabbasi, and Mu Chiao. "Design and Optimization of Resonance-Based Efficient Wireless Power Delivery Systems for Biomedical Implants". In: *Biomedical Circuits and Systems, IEEE Transactions on* 5.1 (2011), pp. 48–63. ISSN: 1932-4545. DOI: 10.1109/TBCAS.2010.2072782.

[4] M. Kiani, Uei-Ming Jow, and M. Ghovanloo. "Design and Optimization of a 3-Coil Inductive Link for Efficient Wireless Power Transmission". In: *Biomedical Circuits and Systems, IEEE Transactions on* 5.6 (2011), pp. 579–591. ISSN: 1932-4545. DOI: 10.1109/TBCAS.2011.2158431.

[5] M.W. Baker and R. Sarpeshkar. "Feedback Analysis and Design of RF Power Links for Low-Power Bionic Systems". In: *Biomedical Circuits and Systems, IEEE Transactions on* 1.1 (2007), pp. 28–38. ISSN: 1932-4545. DOI: 10.1109/TBCAS.2007.893180.

[6] R.D. Middlebrook. "Low-entropy expressions: the key to design-oriented analysis". In: *Frontiers in Education Conference, 1991. Twenty-First Annual Conference. 'Engineering Education in a New World Order.' Proceedings.* 1991, pp. 399–403. DOI: 10.1109/FIE.1991.187513.

[7] R.D. Middlebrook. "Null double injection and the extra element theorem". In: *Education, IEEE Transactions on* 32.3 (1989), pp. 167–180. ISSN: 0018-9359. DOI: 10.1109/13.34149.

[8] R.D. Middlebrook. “The general feedback theorem: a final solution for feedback systems”. In: *Microwave Magazine, IEEE* 7.2 (2006), pp. 50–63. ISSN: 1527-3342. DOI: 10.1109/MMW.2006.1634022.

[9] C.M. Zierhofer and E.S. Hochmair. “The class-E concept for efficient wide-band coupling-insensitive transdermal power and data transfer”. In: *Engineering in Medicine and Biology Society, 1992 14th Annual International Conference of the IEEE*. Vol. 2. 1992, pp. 382–383. DOI: 10.1109/IEMBS.1992.5761022.

[10] C.M. Zierhofer and Erwin S. Hochmair. “High-efficiency coupling-insensitive transcutaneous power and data transmission via an inductive link”. In: *IEEE Trans. on Biomedical Engineering* 37.7 (1990), pp. 716–722. ISSN: 0018-9294. DOI: 10.1109/10.55682.

[11] Dukju Ahn and Songcheol Hong. “Wireless Power Transmission With Self-Regulated Output Voltage for Biomedical Implant”. In: *IEEE Trans. on Industrial Electronics* 61.5 (2014), pp. 2225–2235. ISSN: 0278-0046. DOI: 10.1109/TIE.2013.2273472.

[12] Frederick Emmons Terman. *Radio engineers’ handbook*. New York; London: McGraw-Hill, 1943.